Bioactivity and mineralization of natural hydroxyapatite from cuttlefish bone and Bioglass® co-sintered bioceramics

Natascia Cozza[1], Felipe Monte[2], Walter Bonani[1,3], Pranesh Aswath[2], Antonella Motta[1,3], Claudio Migliaresi[1,3]

[1] *BIOtech Research Center and European Institute of Excellence on Tissue Engineering and Regenerative Medicine, Department of Industrial Engineering, University of Trento, Trento, Italy*

[2] *Materials Science and Engineering Department, University of Texas at Arlington, TX, U.S.A.*

[3] *INSTM - Consorzio Interuniversitario Nazionale per la Scienza e Tecnologia dei Materiali, Firenze, Italy*

Corresponding author:

Antonella Motta, Department of Industrial Engineering and BIOtech Research Center, University of Trento, Via Sommarive 9, 38123. Trento, Italy

Email: antonella.motta@unitn.it

This article has been accepted for publication and undergone full peer review but has not been through the copyediting, typesetting, pagination and proofreading process which may lead to differences between this version and the Version of Record. Please cite this article as doi: 10.1002/term.2448

Abstract

In this study, bioactive hydroxyapatite-based bioceramics starting from cuttlefish bone powders have been prepared and characterized. In particular, fragmented cuttlefish bone was co-sintered with 30 wt% of Bioglass®-45S5 to synthesize hydroxyapatite-based powders with enhanced mechanical properties and bioactivity. Commercial synthetic hydroxyapatite was treated following the same procedure and used as a reference. The structure and composition of the bioceramics formulations were characterized using Fourier transform infrared spectroscopy, X-ray diffraction and scanning electron microscopy. After the thermal treatment of cuttlefish bone powder added with 30% wt. Bioglass®, new phases with compositions of sodium calcium phosphate ($Na_3Ca_6(PO_4)_5$), β-tricalcium phosphate (β-TCP, $Ca_3(PO_4)$) and amorphous silica were detected.

In vitro cell culture studies were performed by evaluating proliferation, metabolic activity and differentiation of human osteoblast-like cells (MG63).

Scaffolds made with cuttlefish bone powder exhibited increased apatite deposition, ALP activity and cell proliferation compared to commercial synthetic hydroxyapatite. In addition, the ceramic compositions obtained after the combination with Bioglass® further enhanced the metabolic activity of MG63 cell and promoted the formation of a well-developed apatite layer after 7 days of incubation in DMEM.

1. Introduction

Several bioactive ceramics have been proven to be attractive candidates as scaffold materials for bone tissue engineering (Stevens, 2008). In particular, among largely used bioceramics, calcium phosphates based materials are preferred as bone graft materials due to their biocompatibility and chemical similarity to the inorganic matrix

of natural bone (Habraken *et al.*, 2016). Different phases and form of calcium phosphates, including hydroxyapatite (HAP), β-tricalcium phosphate (β-TCP), α-tricalcium phosphate (α-TCP), biphasic calcium phosphate (BCP), and monocalcium phosphate monohydrate (MCP) are currently used in the biomedical industry depending on the physical properties that are required for the specific application (Wang *et al.* 2014).

Hydroxyapatite (HAP, $Ca_{10}(PO_4)_6(OH)_2$) is an ideal phase for applications in human body and has been widely studied for restoration of damaged hard tissue due to its osteoconductivity, bioactivity and chemical stability under physiological pH (Yoshikawa, 2005)(Zhou & Lee, 2011). However, despite the chemical similarity with the mineralized bone of human tissue, the biological properties of synthetic hydroxyapatite significantly differ from those of natural bone. In fact, the mineral phase of bone has a complex composition that besides calcium phosphate comprises carbonate ions, magnesium, sodium, hydrogen phosphate ions and several other trace elements (Ivankovic *et al.*, 2010). The biological outcome of HAPs is strongly related to their composition and, in particular, the presence of various trace elements play a crucial role in the overall physiological functioning and in the osseointegration process (Oryan *et al.*, 2014).

Various natural source materials have been considered for biomedical applications (Malafaya et al., 2007), such as collagen (Chattopadhyay et al. 2014) (Cozza et al. 2016), chitosan (Oliveira et al. 2011), or silk (Motta et al. 2016). Other than for polymers, marine organisms (ex. cuttlefish, corals, jellyfishes, and nacres)(Kim et al., 2012)(Silva et al., 2012)(Sewing et al., 2015)(Felicio-Fernandes et al., 2000), and marine-derived food-waste (Abdulrahman et al., 2014) (Venkatesan et al., 2015) are receiving increasing interest as calcium bio sources because of the possibility to

convert their calcium carbonate structures in hydroxyapatite via a hydrothermal reaction (Vecchio *et al.*, 2007) (Tkalčec *et al.*, 2014).

Cuttlefish mantle is a suitable source of collagen (Cozza et al. 2016), the bone (CF_b), being a source of calcium phosphate (Tkalčec *et al.*, 2014). CF_b, that has a mineral composition compatible with human bone tissue (Rocha *et al.,* 2005) (Ivankovic *et al.,* 2010), is easily available and cheap, being usually a food-waste. Previous studies have demonstrated calcium carbonate structure of CF_b can be converted into hydroxyapatite by using a hydrothermal transformation (Rocha *et al.* 2005) (Tkalčec et al., 2014).

Hydroxyapatite obtained from natural sources is non-stoichiometric and can incorporate other ions, for example CO_3^{2-}, traces of Fe^{2+}, Na^{+}, Mg^{2+}, F^{-} and Cl^{-} (Yoshikawa, 2005), resulting therefore more similar to HAP of natural bone than the stoichiometrically pure hydroxyapatites (Zhou & Lee,2011), and therefore more bioactive (Ivankovic *et al.*, 2010). A limitation of pure hydroxyapatite are the poor mechanical properties that have restricted the use to low-loaded applications. In order to overcome these disadvantages hydroxyapatite has been combined with various ceramic, polymer or metallic reinforcements (Suchanek & Yoshimura, 1998). In addition, the conventional calcium phosphate powders are difficult to sinter, probably because of their low specific surface area (typical 2–5 m^2/g) (Kalita *et al.*, 2004). For these reasons, synthetic hydroxyapatite is sometimes added with a secondary phase as sintering aid to increase densification, such as bioglass (Demirkiran *et al.*, 2010) or other sintering additives containing trace amounts of calcium oxide (Kalita *et al*., 2004). Sintering of hydroxyapatite/bioactive glass mixtures resulted in bioceramics with improved mechanical and biological properties (Lin *et al.*, 1994). The reaction between hydroxyapatite and bioactive glasses

depends on time and temperature of the sintering process, but also on glass composition, each system therefore requiring in depth independent studies.

Among bioactive glasses, Bioglass®-45S5 (consisting of 45 wt.% SiO_2, 24.5 wt.% Na_2O, 24.5 wt.% CaO, and 6 wt.% P_2O_5) has been combined with hydroxyapatite either as a sintering aid or second phase (Gerhardt & Boccaccini, 2010). Previous studies have shown that Bioglass®-45S5 enhances the bioactivity of HAP and generates new ceramic phases, that increase apatite deposition and osteoblast proliferation and differentiation *in vitro* (Demirkiran *et al.*, 2010).

In the present study, for the first time, calcium phosphate powders are synthesized starting from cuttlefish bone powder and at the same time co-sintered with Bioglass®-45S5 at 900°C, in order to develop ceramic compositions that present enhanced bioactivity, osteoconductivity and improved mechanical properties. The structure and composition of the new material were examined using Fourier transform infrared spectroscopy, X-ray diffraction and scanning electron microscopy. Mechanical properties were evaluated using compression tests. In addition, human osteoblast-like cells (MG63) were cultured on these substrates and the cell activity and proliferation, after 1, 3 and 7 days cell culture, were investigated using PicoGreen® DNA quantification, Alamar Blue® and alkaline phosphate activity assays.

2. Materials and Methods

2.1. Materials

Synthetic hydroxyapatite powder (≥ 97 wt.%, particle size < 44 µm) with chemical composition $Ca_{10}(PO_4)_6OH_2$ was acquired from Sigma-Aldrich (St. Louis, MO, USA). Bioglass®-45S5 powder consisting of 45 wt.% SiO_2, 6 wt.% P_2O_5, 14.5 wt.% Na_2O,

and 24.5 wt.% CaO was purchased from US Biomaterials Corporation (Alachua, FL, USA) with particle size < 90 µm.

All the chemicals and reagents used were of analytical grade and without further modifications.

2.2. Cuttlefish powder preparation

Native cuttlefish bones of *S. officinalis* from the Adriatic Sea were cut in small pieces and treated at 300°C for 3 h, to remove the organic component. For the thermal treatment only the internal lamellae part of the bone was used, since the aragonite of the external shell during the pre-treatment at 300°C could partially transform into calcite, which is more difficult to convert into hydroxyapatite (Ivankovic *et al.*, 2010). After thermal treatment, bones were ground into a fine powder (particle size < 100 µm).

2.3. Samples production

Four different groups of scaffolds were produced, using commercial hydroxyapatite powder (sample HAP_st), cuttlefish bone powder (sample CF_p) and their mixtures with 30% wt. of Bioglass®45S5 (samples HAP30B and CF30B)

Briefly, the HAP and cuttlefish bone powders were ball milled with zirconia (Y-TZP) for 48h in 250 ml polyethylene bottles containing 0.6 M aqueous solution of $NH_4H_2PO_4$ (Ca/P = 1.67). For the formulation of samples HAP30B and CF30B, prior to drying 30% wt. of Bioglass®45S5 powders were added and the mixtures were ball milled for another 48 h. All samples were then pressed in a die 6.7 mm diameter,

sintered at 900°C for 3 h with a heating rate of 10°C/min, then cooled to room temperature at 10°C/min.

2.4 Material characterization

2.4.1. Fourier transform infrared spectroscopy (FT-IR)

Fourier transform infrared (FT-IR) spectra of sintered bioceramic mixtures were collected using the Spectrum One spectrometer with ATR correction (Perking Elmer, Waltham, MA, USA) with Zinc Selenide crystal. Sample spectra were averaged over 4 scans, ranging from 600 to 3000 cm^{-1} at a resolution of 4 cm^{-1}.

2.4.2. X-ray diffraction (XRD) analyses

X-ray diffraction analysis of sintered bioceramic mixtures was performed with a Bruker D8 Advance X-ray diffractometer using CuK_{α} radiation. The data were recorded over the 2ɵ range of 20-60° with a 0.04° step size and a dwell time of 1 s.

2.4.3. Scanning Electron Microscopy with X-ray microanalysis (SEM/EDXS)

The microstructures of the bioceramic samples after sintering and subsequent cell culture studies were investigated using Hitachi S-300N VP-SEM and Supra 40 Zeiss scanning electron microscopes operated in high vacuum and secondary electron mode. The composition of samples was examined through energy-dispersive X-ray spectroscopy (EDXS) (Nova NanoSEM 450, FEI, Hillsboro, OR, USA).

2.4.4. Compression tests

The compression tests were performed at a crosshead speed of 1 mm/min with a Bose ElectroForce® AT 3300 servo electric material test machine (TA Instruments,

Eden Prairie, MN, USA) on four samples for each bioceramic composition. Samples prepared according to ASTM C773-88 (2006) were cylinders 12 mm high and 6 mm diameter. Compressive strength was evaluated as the ratio between the load to failure and the samples cross-sectional area

2.5. *In vitro* biological evaluation

The mineralization and more specifically the deposit of apatite on the surfaces of the different bioceramics formulations was evaluated with SEM analysis after 7 days incubation of samples in Dulbecco's Modified Eagle's medium (DMEM) (Euroclone, Milan, Italy) without cells [Lee *et al.*, 2011].

2.5.1. Cell culture

MG63 cells (human osteosarcoma cells line) were used to assess the in vitro biocompatibility of the different bioceramics formulations. Cells were expanded and cultured at 37ºC with 5% CO_2 in Dulbecco's Modified Eagle's medium (DMEM) (Euroclone, Milan, Italy) containing 10% fetal bovine serum (Gibco, NY, USA), supplemented with 1mM sodium pyruvate, 2 mM L-glutamine, 0.1% antibiotics (Gibco, Eggenstein, Germany). Culture medium was changed every 2 days until cells confluence, and then cells were detached from the culture plate with 0.1% trypsin and re-suspended in the culture medium. Prior to cell seeding, bioceramics samples for cell tests were sterilized in 70% ethanol for 3 hours and pre-conditioned with DMEM for 2 hours. MG63 cells were finally seeded on the samples individually kept in a 96-well polystyrene plate, at a density of 7×10^3 cells per well, and incubated under standard culture conditions.

2.5.2. Cell morphological characterization by Confocal Laser Scanning Microscopy (CLSM)

After 1, 3 and 7 days of culture, the cells were fixed, permeabilized with 4% paraformaldehyde solution in PBS with 0.2% Triton X-100, then labeled with Rhodamine phalloidin (Molecular Probes®, Life Technologies, Monza, Italy) for the visualization of filamentous actin (F-actin) and 4',6-Diamidino-2-Phenylindole, Dilactate (DAPI, Molecular Probes®) to stain the nuclei. The morphology of the cells adhered to the substrate was observed by Nikon A1 confocal laser microscopy (Nikon Instruments, Florence, Italy).

2.5.3. Cell proliferation by DNA quantification

To evaluate cell proliferation on the bioceramics samples, a PicoGreen® DNA quantification assay (Quant-iT PicoGreen® dsDNA Assay, Invitrogen™, Carlsbad, USA) was used. At 1, 3 and 7 days, the culture medium was removed and the samples were washed with PBS. Samples were then covered with 300 µL of 0.05% Triton-X in PBS, and the supernatants were collected and stored in single vials at -20°C until analysis. Before analysis, vials were thawed at room temperature, and sonicated for 10 seconds with a Hielscher ultrasonic homogenizer (UP400S, 400 watt-24 kHz, amplitude 50%, from Hielscher Ultrasonics, Teltow, Germany). Extracts of 100 µL were subsequently placed in a black 96-well plate, and mixed with 100 µL of PicoGreen® working solution, prepared following the manufacturer's instructions. Five independent samples were analyzed for each experimental condition. Fluorescence intensity was measured with a Tecan Infinite 200 microplate reader (Tecan Group, Männedorf, Switzerland) using excitation wavelength 485 and emission wavelength 535 nm. A calibration curve was created using a double-

stranded DNA standard provided by the kit and was used for the calculation of the DNA content. Finally, the approximate number of cells per sample was determined from DNA content by the conversion factor of 7.7 pg DNA per cell.

2.5.4. Cell metabolic activity (AlamarBlue® assay)

Cells viability after 1, 3 and 7 days of culture was determined with AlamarBlue® Cell Viability assay (Invitrogen™, Carlsbad, USA), that quantifies cellular metabolic activity and in turn determines the concentration of viable cells in a given sample. AlamarBlue® reagent was added directly to each well 10% of the cell culture medium volume. Then, the well plates were incubated at 37°C in a humidified atmosphere with 5% CO_2 for 2 hours. A volume 100 µL of solution was collected from each well and the fluorescence signal was measured with a Tecan Infinite 200 microplate reader (Tecan Group, Männedorf, Switzerland) with an excitation wavelength of 560 nm and an emission wavelength of 590 nm. Five replicated were considered for each experimental condition.

2.5.5. Alkaline phosphatase activity

The functional activity of the proliferated cells was determined with a Alkaline Phosphatase Fluorometric Assay Kit (Abcam, Cambridge, UK). At 1, 3 and 7 days of culture, the scaffolds were washed with PBS, and incubated with 300 µL of cell lysis buffer containing 0.2% Triton X-100 for 30 min. Then, the supernatants were collected and stored at -20°C. Samples were thawed before the analysis to room temperature and the ALP test was run following the manufacturer's instructions. Fluorescence intensity was measured with a Tecan Infinite 200 microplate reader (Tecan Group, Männedorf, Switzerland) using excitation wavelength of 360 nm and emission wavelength of 440 nm. Five samples were analyzed for each experimental

condition. The ALP activity was calculated from a standard curve, which was generated using the reagents provided with the commercial kit.

2.6. Statistics

The *in vitro* MG63 cell proliferation and differentiation tests were performed on five replicates for each group of bioceramic compositions. All quantitative data were expressed as mean ± standard deviation (SD). Statistical analyses were performed using GraphPad Prism 5 (GraphPad Software, La Jolla, CA, USA). The quantitative mechanical and biological results were compared using a one-way analysis of variance (ANOVA); Tukey's HSD (honest significant difference) post hoc test was applied to determine specific differences among groups after testing for homogeneity of variances. Unless otherwise specified, a significance level of 95% with a p value of 0.05 was used in all statistical tests performed. Equality of variances was verified before applying the tests.

3. Results

3.1. Physical and chemical characterization

A scanning electron micrograph of the inner structure of the cuttlefish bone is reported in Fig. 1a. Cuttlefish bone presented a unique microstructure characterized by layered regular sheets, with lamellar spacing ranging from 100 to 300 µm. Pieces of about 1 x 1 x 2 cm^3 were cut from the internal bone matrix, treated at 300°C to remove the organic component, and mechanically fragmented. The powder obtained after the ball milling of the cuttlefish bone consisted of flake-like particles, with irregular shape and size ranging from 10 to 20 µm (Fig. 1b). The EDXS spectrum

and XRD analysis of the cuttlefish bone powder (Fig. 1c and Fig. 1d) confirmed the inorganic component of the starting material as crystalline $CaCO_3$ in the form of pure aragonite (Rocha *et al.*, 2005). In particular, the XRD analysis clearly demonstrated that the relative intensity of the peaks of cuttlefish bone powder matches with the standard aragonite, while significantly differs from the standard calcite, plotted at the bottom side of the diagram. These results proved that the lamellae matrix of cuttlefish bone retained the aragonitic structure after the pre-treatment at 300°C.

The aragonitic structure of cuttlefish bone powder was converted in HAP after 90 minutes of thermal treatment at 900°C. The conversion of aragonite into hydroxyapatite powder was followed by FT-IR spectroscopy (Fig.2 a) and XRD analysis (Fig.2 b). The results clearly showed that the characteristic bands of the functional groups of hydroxyapatite phase are absent in the FT-IR and XRD spectra of cuttlefish powder. After thermal treatment, the FT-IR of the powder presented the characteristic peak of hydroxyapatite around 1021 cm^{-1}, assigned to the vibrations of phosphate groups (Rehman & Bonfield, 1997). The characteristic peaks of hydroxyapatite can be detected also in the XRD spectra of the powder after the thermal treatment. In particular the three peaks of HAP at $2\theta = 25.8°$ (0 0 2), 31.7° (2 1 1), and 32.9° (3 0 0) are present (Ślósarczyk *et al.*, 2005).

Fig. 3 shows the XRD patterns of the samples produced using commercial hydroxyapatite and cuttlefish bone powders, containing 30 wt.% of Bioglass®45S5, after the thermal treatment at 900°C for a period of 3 hours.

When 30 wt.% Bioglass®45S5 are added to the cuttlefish powders (samples CF30B), the phases detected after the thermal treatment at 900°C are hydroxyapatite, sodium calcium phosphate ($Na_3Ca_6(PO_4)_5$, JCPDS#40-0393) and β-TCP ($Ca_3(PO_4)$, JCPDS#09-0169). In this case there is no evidence of any crystalline silicate phases.

However, when 30 wt.% Bioglass®45S5 are added to the commercial synthetic hydroxyapatite powders and treated at 900°C (samples HAP30B) the main phases present in the product seem to be hydroxyapatite and $Na_2Ca_2Si_2O_7$ (JCPDS#10-0016).

The EDXS element mapping analyses of the samples containing 30% wt. Bioglass®45S5, after the thermal treatment at 900°C, are reported in Fig. 4. The Grey images in the figure are the base image of the local regions used for the EDXS mapping of the samples, while the colored images show the corresponding O, Ca, P, Na and Si element mapping in the same regions. In both samples, O, Ca and P are evenly distributed throughout the entire region, while silicon is localized in specific areas of the surface. However, is interesting to note that, in the samples CF30B, silicon is localized in Ca deficient areas of the surface and it seems not combined with other elements to form new phases after the treatment at 900°C. However, the element mapping of the samples HAP30B showed that, in this case, silicon is combined with Ca and Na, suggesting the presence of calcium silicate compounds in some areas of the surface.

3.2. Mechanical property characterization

The compressive stress-strain curves and the ultimate compressive strength of the different sintered samples are shown in Fig. 5.

Samples CF30B and HAP30B presented the highest compressive strength values proving that the addition of Bioglass®45S5 significantly improves the average compressive strength of the sintered bioceramic samples.

3.3. In vitro biological characterization

In order to investigate the deposition of apatite on the surfaces of the different bioceramics formulations, samples were placed for 7 days in media without cells. After 7 days of immersion in the culture media, all the samples presented an apatite layer and in particular samples containing Bioglass® (HAP30B and CF30B), had the largest amount of apatite formation (Fig. 6).

3.3.4 Cell adhesion, morphology and distribution

As shown in Fig.7, the actin microfilament cytoskeleton and nucleus of cells after 1, 3 and 7 days of cells culture were stained to visually explore the adhesion and spreading of MG63 cells on the different samples. At day 1, rhodamine-phalloidin and DAPI staining revealed a comparable number of cell attachment on all the samples. However, in the sample CF_p, cytoskeleton organization was not very prominent in comparison with the other samples formulations. After three days of cell culture, the cell started to growth and showed a stretched morphology of the cytoskeleton arrangement. At day 7, an appreciable cellular growth was evident in all the samples. In particular, samples CF_p and CF30B presented a significant increase in cells number; the entire surface of the substrates appeared to be covered by a continuous carpet of spread cells with well-organized actin filaments and well-developed cytoskeleton.

3.3.1. Cell proliferation by DNA quantification

To investigate the ability of the different bioceramic formulations to promote cell proliferation and growth, MG63 cells were seeded on the scaffolds, and their behavior was subsequently investigated. Cell proliferation studies were performed at different time points over a period of 7 days (Day 1, Day 3 and Day 7), using the PicoGreen® DNA quantification assay. According to the results (Fig. 8a), the cell

number increased gradually at each time point and reached for all the samples its peak on day 7. At day 7, the samples produced using the cuttlefish bone powder as starting material (samples CF_p and CF30B) presented a significantly higher cell number in comparison with the samples HAP_st and HAP30B.

These findings are in agreement with the confocal results that evidenced a larger cell growth for the scaffolds produced from the cuttlefish bone powder than for those produced with the commercial stoichiometric HAP.

3.3.2. Cell metabolic activity by AlamarBlue® assay

Fig. 8b and Fig. 8c show the metabolic activity, measured using AlamarBlue® assay, of MG63 cells cultured for 1, 3 and 7 days on samples produced with the different formulations. For all the substrates the cellular metabolic activity of the systems continued to increase up to 7 days of culture (Fig. 8b). At day 7, cells seeded on samples containing Bioglass®-45S5 (HAP30B and CF30B) showed a significantly higher total metabolic activity when compared to the substrates prepared without the addition of the Bioglass (HAP_st and CF_p). Total cell metabolic activity was also normalized to the total DNA content previously determined using the PicoGreen® DNA quantification assay. Normalized metabolic activity values are presented in Fig. 8c. Interestingly, cells seeded on HAP30B substrates showed a higher specific activity when compared to cells seeded in HAP_st samples at all time points. On the other side, the CF-based substrates (CF_p and CF30B) showed a lower normalized activity than the HAP-based counterparts at day 7.

3.3.3. Alkaline phosphatase activity

The production of intracellular alkaline phosphatase (ALP) of MG63 cell line was monitored at 1, 3 and 7 days (Fig. 8d). Interestingly, CF30B was the only substrate demonstrating an early ALP production at day 3. Similarly, sample CF30B showed

the highest value for ALP activity among all the experimental groups both at day 3 and at day 7. In addition, CF-based samples (both CF_st and CF30B) displayed higher ALP production when compared to HAP-based substrates at day 7. The plot in Fig. 8e reports the ALP activity normalized to previously determined DNA content. Also in this case, sample CP30B presented the highest value of normalized ALP activity at day 3. At day 7, no differences in terms of normalized ALP production were found between the samples containing Bioglass®-45S5 (HAP30B and CP30B) at day 7.

4. Discussion

Among the requirements for scaffolds materials in bone tissue engineering applications, bioactivity and osteoconductivity are crucial aspects to achieve successful tissue regeneration. At the same time, the mechanical properties of the scaffold are critical in order to support the loads during the regeneration process.

Hydroxyapatite is the major mineral component of native bone and it has been widely used in several bone tissue engineering applications. However, it is well known that hydroxyapatite cannot be used alone as scaffold material because of its poor mechanical properties (Wang, 2003).

As previously suggested in literature, strong chemical bonds can be formed during the sintering process of hydroxyapatite/bioactive glass formulations and the presence of a glassy phase can promote the decomposition of hydroxyapatite to β-TCP, thus accelerating atomic diffusivity and the kinetics of the sintering process (Chatzistavrou *et al.*, 2006). As a consequence, hydroxyapatite-based structures with enhanced mechanical properties can be obtained by sintering hydroxyapatite/bioactive glass powder formulations (Goller *et al.*, 2003).

In addition, it has been demonstrated that the cosintering process can induce the formation of new ceramic phases. In particular, Demirkiran *et al.* have reported that the sintering process of hydroxyapatite with 10 wt.% Bioglass®45S5 resulted in the formation of calcium phosphate silicate ($Ca(PO_4)_2SiO_4$) and limited amount of β-TCP, while the composition with 25 wt.% Bioglass®45S5 originated sodium calcium phosphate ($Na_3Ca_6(PO_4)_5$) with no evidence of β-TCP (Demirkiran *et al.*, 2010).

Our results confirmed that the samples containing Bioglass®45S5 (HAP30B and CF30B) exhibited a significantly higher compressive strength when compared with those produced without Bioglass® (HAP_st and CF_p). At this regard, a further improvement of the compressive strengths of the samples could be achieved thought the optimization of the process parameters. For example previously studies have indicated that the compressive strengths increase significantly using powders with uniform particle sizes distribution, high pre-sintering compaction pressure and when the sintering temperature is higher than 1200°C (Prokopiev & Sevostianov, 2006).

In this study we have demonstrated that the addition of 30 wt.% Bioglass®45S5 to the HAP (HAP30B) trigged the decomposition of commercial stoichiometric hydroxyapatite during sintering at 900°C into CaO and β-TCP, that further reacted with the Bioglass® with the formation of new phases. In particular, the XRD analysis of HAP30B demonstrated the formation of both hydroxyapatite and $Na_2Ca_2Si_2O_7$ (40.9 wt% SiO_2, 38.3 wt% CaO, 20.8% wt Na_2O) after sintering. Furthermore, the element mapping of these samples showed that silicon was combined with Ca and Na and indicated the presence of calcium silicate compounds in some areas of the surface.

On the other hand, the XRD analysis of sample CF30B did not reveal the presence of any crystalline silicate phase. This is probably related to the fact that for this

formulation hydroxyapatite was generated through the thermal conversion of aragonite ($CaCO_3$) structure of CF powder, following the chemical reaction: $10CaCO_3 + 6(NH_4)_2HPO_4 + 2H_2O \rightarrow Ca_{10}(PO_4)_6(OH)_2 + 6(NH_4)_2CO_3 + 4H_2CO_3$ (Rocha *et al.*, 2005).

At the same time, $CaCO_3$ was thermally decomposed to obtain CaO that reacted with P_2O_5 provided by Bioglass® to form β-TCP. The further incorporation of Na^+ cations into the structure resulted in the formation of $Na_3Ca_6(PO_4)_5$. It is interesting to note that the elements mapping of CF30B indicated that silicon was localized in Ca-deficient areas of the surface, thus suggesting that silica segregated as amorphous silica in localized regions of the samples surface during the thermal treatment.

In vitro biological evaluation was performed to investigate the effect of the new chemistry on the cellular response. MG63 cell line was used to evaluate the biocompatibility of the different bioceramics formulations. These cells are derived from a human osteosarcoma and are frequently used as an experimental model to study different osteoblast functions. In fact, these cells present a number of features typical of an undifferentiated osteoblast phenotype, including the synthesis of collagen type I and III, production of osteocalcin and the expression of alkaline phosphatase (Clover & Gowen, 1994).

We have demonstrated that the scaffolds based on cuttlefish bone powder (samples CF_p and CF30B) stimulated MG63 cells proliferation after 7 days of *in vitro* culture. In fact, analysis of DNA content and confocal images demonstrated a significant enhancement of the cell number, and a higher cellular proliferation for cuttlefish bone derived samples (CF_p and CF30B) in comparison with samples produced using the commercial synthetic hydroxyapatite (Fig. 8a). We also noticed that the formation of new phases in the formulations with Bioglass® significantly influenced the cell activity

(Fig. 8b). This enhancement of the metabolic activity in the samples CF30B and HAP30B is consistent with previous works that studied the behavior of bioceramic surfaces in presence of Bioglass®. In particular, Clark *et al.* reported that silica gel layer is formed on the surface of bioceramics as a result of Bioglass® partial dissolution (Clark *and al.*, 1976). Such newly formed silica layer promotes cell proliferation and differentiation and at the same time improves the mineralization process through the formation of an apatite layer. Moreover, it has been shown that formulations containing bioactive glasses release silicon, calcium, sodium and phosphate ions during the degradation in the physiological conditions. Such ions are important because Ca, Si and P are the main components of biological apatite and play a crucial role in bone formation and resorption (Ducheyne & Qiu, 1999). In particular, Ca is involved in the activation of the intracellular mechanisms during bone remodeling and Si is implicated in the metabolic processes of new bone matrix formation and calcification (Hoppe *et al.*, 2011). Therefore, the dissolution products of bioactive glasses can stimulate cells to produce new bone tissue and, at the same time, improve the mineralization process. Interestingly, the formulations containing Bioglass® were shown to promote the cell activity to a greater extent than the Bioglass-free substrates, even when normalized activity was taken into consideration (Fig. 8c). We also found that cells seeded on substrates based on cuttlefish bone powder (samples CF_p and CF30B) presented a reduction in normalized activity at day 7. However, as revealed by confocal examination at day 7 samples CF_p and CF30B had already reached a confluence state and the reduction in single-cell metabolic activity could be related to contact inhibition phenomena.

In this study, SEM analysis indicated calcium deposition on all the scaffolds after 7 days of immersion in DMEM and a highly developed apatite layer, in particular for

the samples containing Bioglass®. In the sample CF30B, the dissolution of amorphous silica on the surface could also contribute to enhance the bioactivity thanks to the release of silicon ions.

However, a suitable model for bone tissue engineering applications requires also that cells be able to differentiate into bone-forming cells. Alkaline phosphate (ALP) is an enzyme that is associated with calcification and its activity increases when osteoblasts produce osteoid. In particular, ALP expression characteristically reaches a maximum level during the phase of matrix maturation, just before mineralization actually begins (Boyan *et al.,* 2011). For this reason, ALP enzyme is considered an early marker of osteoblast differentiation. Furthermore, the ALP enzyme has the effect to increase local levels of inorganic phosphate, one of the components of apatite, revealing the activation of the early phases that will lead to the mineralization process (Delmas, 1993). The ALP measurements of the bioceramics formulations indicated that the CF-based substrates were more effective to promote ALP production than scaffolds produced with commercial stoichiometric hydroxyapatite. It should be noted that no differences were found between HAP30B and CF30B samples at day 7, in terms of normalized ALP activity per cell. However, due to the higher proliferation rate of MG63 cells on the cuttlefish bone-derived substrates, the overall ALP production of the CF30B system was considerably higher. In addition, CF30B sample showed an up-regulation of ALP activity as early as at 3 days from the seeding, entailing an early onset of the osteogenesis process. These results suggest that the chemical composition of the non-stoichiometric hydroxyapatite synthesized from cuttlefish bone, could provide an adequate stimulatory effect on both cell proliferation and differentiation.

6. Conclusions

In this study, a method to produce highly bioactive hydroxyapatite based scaffolds starting from cuttlefish bone powders was studied. In particular, fragmented cuttlefish bone was co-sintered with Bioglass®-45S5 at 900 °C for 3 h, to obtain ceramics compositions with enhanced bioactivity and mechanical properties. The composition and biological properties of the different bioceramics formulations were studied considering potential use of the material for bone tissue engineering applications. The X-ray diffraction analysis of the samples evidenced that the incorporation of the bioactive glass mixture promoted the sintering process and resulted in new phases formation. In particular, the addition of 30 % wt. Bioglass® to the cuttlefish bone powder resulted in the formation of sodium calcium phosphate ($Na_3Ca_6(PO_4)_5$), β-tricalcium phosphate (β-TCP, $Ca_3(PO_4)$) and amorphous silica. The compressive tests of the samples proved that the combination with Bioglass®45S5 increased the mechanical properties of scaffolds. In addition, the biological tests indicated that it positively affected also the *in vitro* metabolic activity of MG63 cells. Furthermore, the samples produced starting from cuttlefish bone powder showed the largest apatite deposition on the surface when immersed in DMEM and the highest proliferation of MG63 cells, after 7 days of cell culture. Finally, the measurements of ALP activity evidenced that naturally derived hydroxyapatite could be effective to promote both, cell proliferation and differentiation. These results make cuttlefish bone a cost-effective and environmentally friendly source of hydroxyapatite and that physical and biological properties can be optimized for bone tissue engineering applications with the addition of Bioglass®.

References

Abdulrahman I., Ibiyeye Tijani H., Abubakar Mohammed B. 2014, From Garbage to Biomaterials: An Overview on Egg Shell Based Hydroxyapatite, *J. Mat*., **2014:** 802467.

Boyan B. D., Lohmann C. H., Dean D. D., et al. 2011, Mechanisms involved in osteoblast response to implant surface morphology, *Annual Rev. Mater. Sci.*, **31**(1): 357–371.

Chattopadhyay, S., Raines, R. T. 2014, Review collagen-based biomaterials for wound healing. *Biopolymers*, **101**: 821–833.

Chatzistavrou X., Chrissafis K., Kontonasaki E., et al. 2006, Sintered Hydroxyapatite/Bioactive Glass Composites : Thermal Analysis and Bioactivity, In: Key Engineering Materials. Trans Tech Publications, eds Nakamura T., Yamashita K., Neo M., Trans Tech Publications, **309-311**: 167–170.

Clark A. E., Pantano C. G., Hench L. L. 1976, Auger spectroscopic analysis of bioglass corrosion films, *J. Am. Cer. Soc.,* **59**(1-2): 37–39.

Clover J., Gowen M. 1994, Are MG-63 and HOS TE85 human osteosarcoma cell lines representative models of the osteoblastic phenotype?, *Bone*, **15**, (6): 585–591.

Cozza N., Bonani W., Motta A., Migliaresi C. 2016, Evaluation of alternative sources of collagen fractions from Loligo vulgaris squid mantle. Int. *J. Biol. Macromol*., **87**, 504-513.

Demirkiran H., Mohandas A., Dohi M., et al. 2010, Bioactivity and mineralization of hydroxyapatite with bioglass as sintering aid and bioceramics with Na3Ca6(PO4)5 and Ca5(PO4)2SiO4 in a silicate matrix, *Mater. Sci. Eng. C*, **30**(2): 263–272

Delmas P.D. 1993, Biochemical markers of bone turnover, *J. Bone Miner. Res*., (8)(S2): S549–S555.

Ducheyne P., Qiu Q. 1999, Bioactive ceramics : the effect of surface reactivity on bone formation and bone cell function, *Biomaterials*, **20**(23): 2287–2303.

Felício-Fernandes G., Laranjeira M.C.M. 2000, Calcium phosphate biomaterials from marine algae. Hydrothermal synthesis and characterization, *Quimica Nova,* **23**(4): 441-6.

Gerhardt L., Boccaccini A. R. 2010, Bioactive Glass and Glass-Ceramic Scaffolds for Bone Tissue Engineering, *Materials*, **3**(7): 3867–3910.

Goller G., Demirkıran H., Oktar F. N., Demirkesen E. 2003, Processing and characterization of bioglass reinforced hydroxyapatite composites, *Ceram. Int*., **29**(6): 721–724.

Habraken W., Habibovic P., Epple M., Bohner M. 2016, Calcium phosphates in biomedical applications: materials for the future?, *Biochem. Pharmacol*., **19**(2); 69–87.

Hoppe A., Güldal N. S., Boccaccini A. R. 2011, A review of the biological response to ionic dissolution products from bioactive glasses and glass-ceramics, *Biomaterials*, **32**(11): 2757–2774.

Ivankovic H., Orlic S., Kranzelic D., Tkalcec E. 2010, Highly Porous Hydroxyapatite Ceramics for Engineering Applicatios, *Adv. Sci. Technol*., **63**: 408–413.

Ivankovic H., Tkalcec E., Orlic S., et al. 2010, Hydroxyapatite formation from cuttlefish bones: kinetics, *J. Mater. Sci. Mater. Med*., **21**(10): 2711–2722.

Kalita S. J., Bose S., Hosick H. L., Bandyopadhyay A. 2004, CaO – P2O5– Na_2O-based sintering additives for hydroxyapatite (HAp) ceramics, Biomaterials, **25**(12): 2331–2339.

Kim B.S. Kim J.S., Sung H-M., et al. 2012, Cellular attachment and osteoblast differentiation of mesenchymal stem cells on natural cuttlefish bone, *J. Biomed. Mater. Res. A*., **100A**(7): 1673–1679.

Lee J., Leng Y., Chow K., et al. 2011, Cell culture medium as an alternative to conventional simulated body fluid, *Acta Biomaterialia*, **7**: 2615-22.

Lin F., Lint C., Liut H., et al. 1994, Sintered porous DP-bioactive glass and hydroxyapatite as bone substitute, *Biomaterials*, **15**(13): 1087-98.

Malafaya P.B., Silva G.A., Reis R.L. 2007, Natural origin polymers as carriers and scaffolds for biomolecules and cell delivery in tissue engineering applications, *Adv. Drug Del. Rev*., **59**: 207-33.

Motta A., Floren M., Migliaresi C. Silks: a unique family of biopolymers. In: “Biomaterials from Nature from Advanced Devices & Therapies”, eds Nuno M. Neves and Rui L. Reis, John Wiley and Sons, Inc., Hoboken, New Jersey. Doi: 10.1002/9781119126218.ch8, 2016, 127-41.

Oliveira, J. T. and Reis, R. L. 2011, Polysaccharide-based materials for cartilage tissue engineering applications, *J. Tissue Eng. Regen. Med*., **5**: 421–436.

Oryan A., Alidadi S., Moshiri A., Maffulli N. 2014, Bone regenerative medicine: classic options, novel strategies, and future directions, *J. Orthop. Surg. Res*., **9**(1): 18.

Prokopiev O., Sevostianov I. 2006, Dependence of the mechanical properties of sintered hydroxyapatite on the sintering temperature, *Mat. Sci. Eng.: A*, **431**(1): 218–227.

Rehman I., Bonfield W. 1997, Characterization of hydroxyapatite and carbonated apatite by photo acoustic FTIR spectroscopy, *J. Mater. Sci. Mater. Med*., **8**(1): 1–4.

Rocha J. H. G., Lemos A. F., Agathopoulos S., et al. 2005, Scaffolds for bone restoration from cuttlefish, *Bone,* **37**(6): 850–857.

Rocha J. H. G., Lemos A. F., Kannan S., et al. 2005, Hydroxyapatite scaffolds hydrothermally grown from aragonitic cuttlefish bones, *J. Mater. Chem*., **15**(47: 5007–5011.

Sewing J., Klinger M., Notbohm H. 2015, Jellyfish collagen matrices conserve the chondrogenic phenotype in two- and three-dimensional collagen matrices. *J Tissue Eng Regen Med,* DOI: 10.1002/term.1993.

Silva T.H., Alves A., Melo Ferreira B., Reis R.L. 2012, Materials of marine origin: A review on polymers and ceramics of biomedical interest, *Inter. Mater. Rev.,* **57**(5):276-306.

Ślósarczyk A., Paszkiewicz Z., Paluszkiewicz C. 2005, FTIR and XRD evaluation of carbonated hydroxyapatite powders synthesized by wet methods, *J. Mol. Struct.,* **744**: 657–661.

Stevens M. M. 2008, Biomaterials for bone tissue engineering, *Mater. Today*, **11**(5): 18–25.

Suchanek W., Yoshimura M. 1998, Processing and properties of hydroxyapatite-based biomaterials for use as hard tissue replacement implants, *J. Mater. Res*., **13**(1): 94–117.

Tkalčec E., Popović J., Orlić S., et al. 2014, Hydrothermal synthesis and thermal evolution of carbonate-fluorhydroxyapatite scaffold from cuttlefish bones*, Mater. Sci. Eng. C. Mater. Biol. Appl.,* 42: 578–86.

Vecchio, X. Zhang, J. B. Massie, et al. 2007, Conversion of bulk seashells to biocompatible hydroxyapatite for bone implants*, Acta Biomater.,* 3(6): 910–918.

Venkatesan J., Kim S-K. 2015, Marine Biomaterials, in: Springer Handbook of marine Biotechnology, ed Kim S-K, XLVI, Springer, Berlin (D), chapter 53: 1-24.

Wang M. 2003, Developing bioactive composite materials for tissue replacement, *Biomaterials*, **24**(13): 2133–2151.

Wang P., Zhao L., Liu J., et al. 2014, Bone tissue engineering via nanostructured calcium phosphate biomaterials and stem cells, *Bone Res*. *2,* 14017.

Yoshikawa H. 2005, Bone tissue engineering with porous hydroxyapatite ceramics, J Artif Organs., 8(3): 131–136.

Zhou H., Lee J. 2011, Nanoscale hydroxyapatite particles for bone tissue engineering, *Acta Biomater.,* **7**(7): 2769–2781.

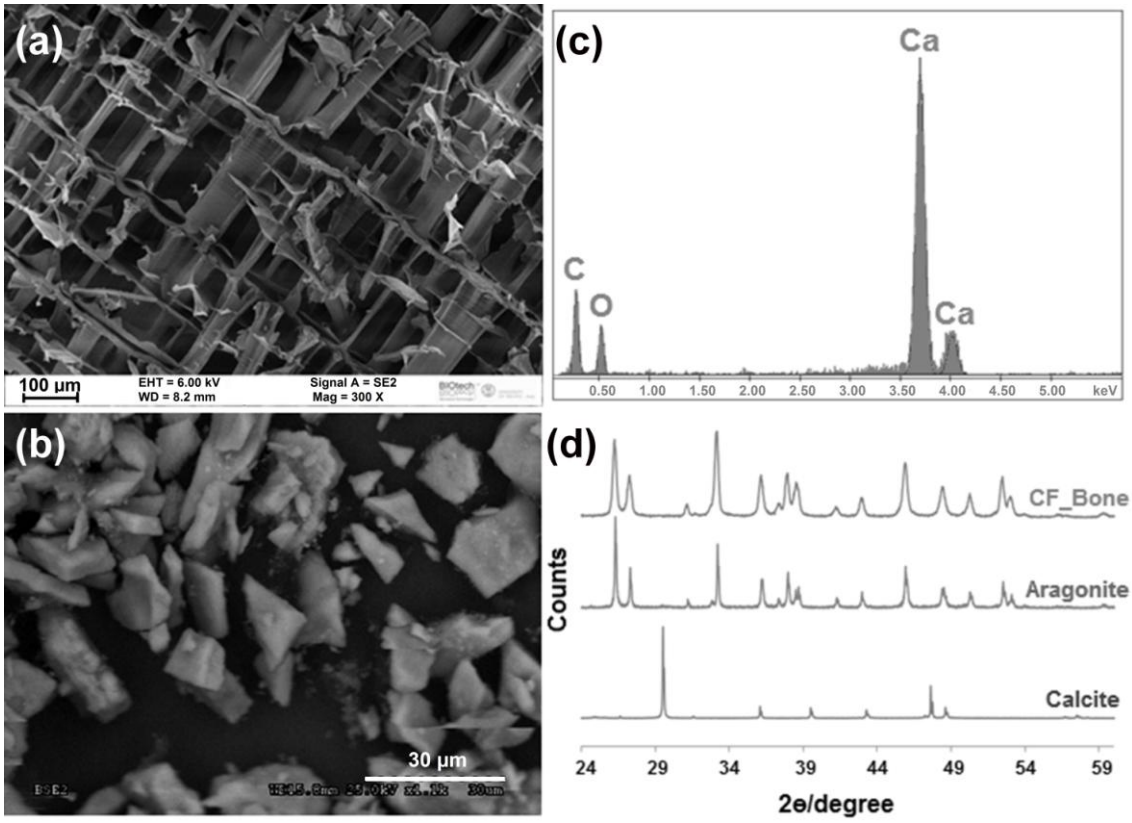

Figure 1. (a) SEM image of the lamellar porous structure of cuttlefish bone; (b) SEM image of the powder obtained after the grinding process of the cuttlefish bone; (c) EDXS spectrum of cuttlefish bone powder; (d) XRD analysis of cuttlefish bone. The figure reports the spectrum of the cuttlefish bone powder in comparison with the spectra of pure Aragonite and Calcite.

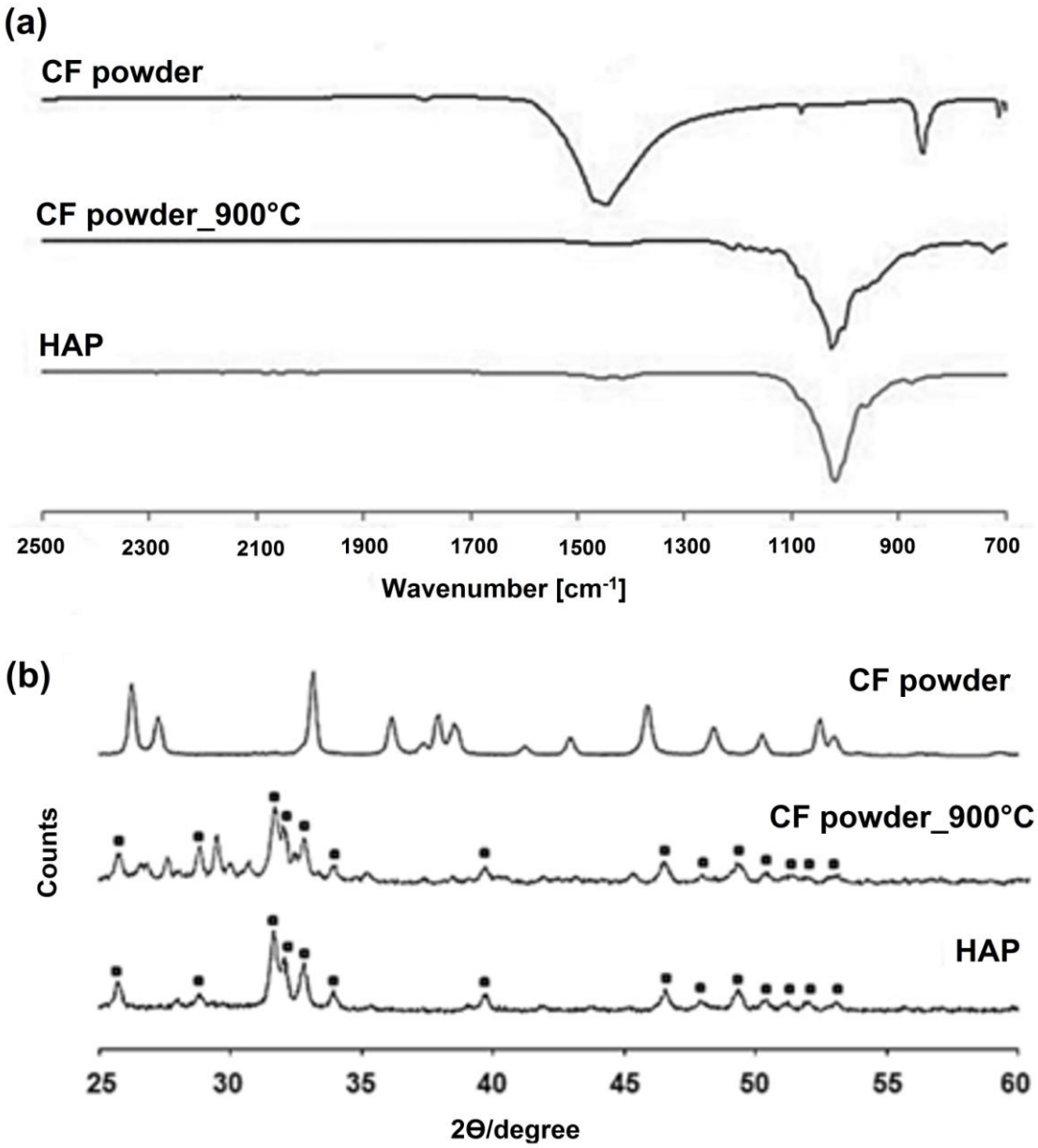

Figure 2. FT-IR (a) and XRD (b) spectra of cuttlefish bone powder before and after 90 minutes of thermal treatment at 900°C in comparison with the spectrum of synthetic hydroxyapatite powder (HAP).

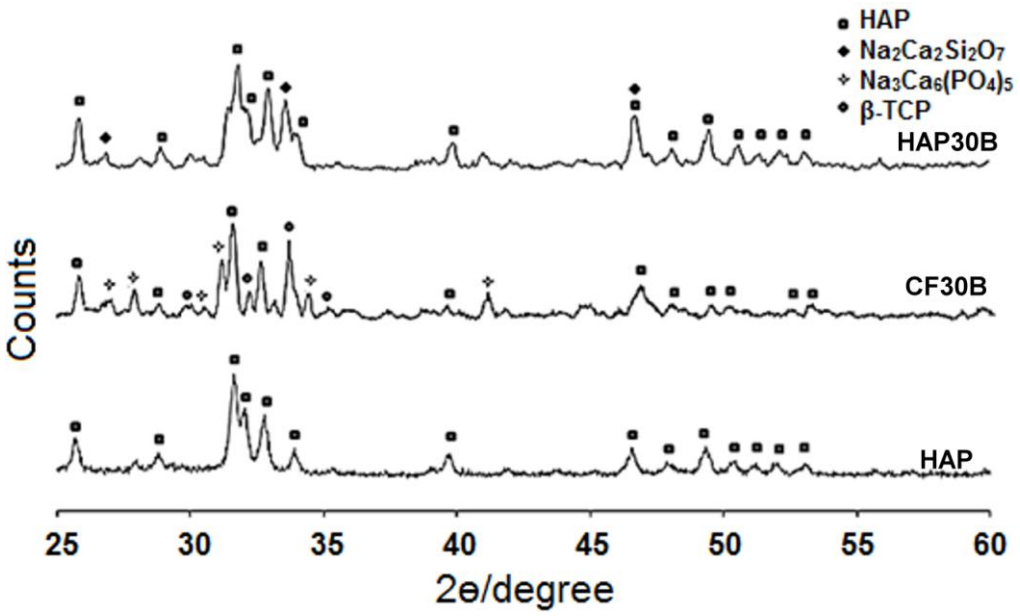

Figure 3. XRD spectra of synthetic hydroxyapatite/Bioglass®45S5 (samples HAP30B) and cuttlefish bone powder/Bioglass®45S5 (samples CF30B) after 3 hours of thermal treatment at 900°C in comparison with the spectrum of synthetic hydroxyapatite powder (HAP).

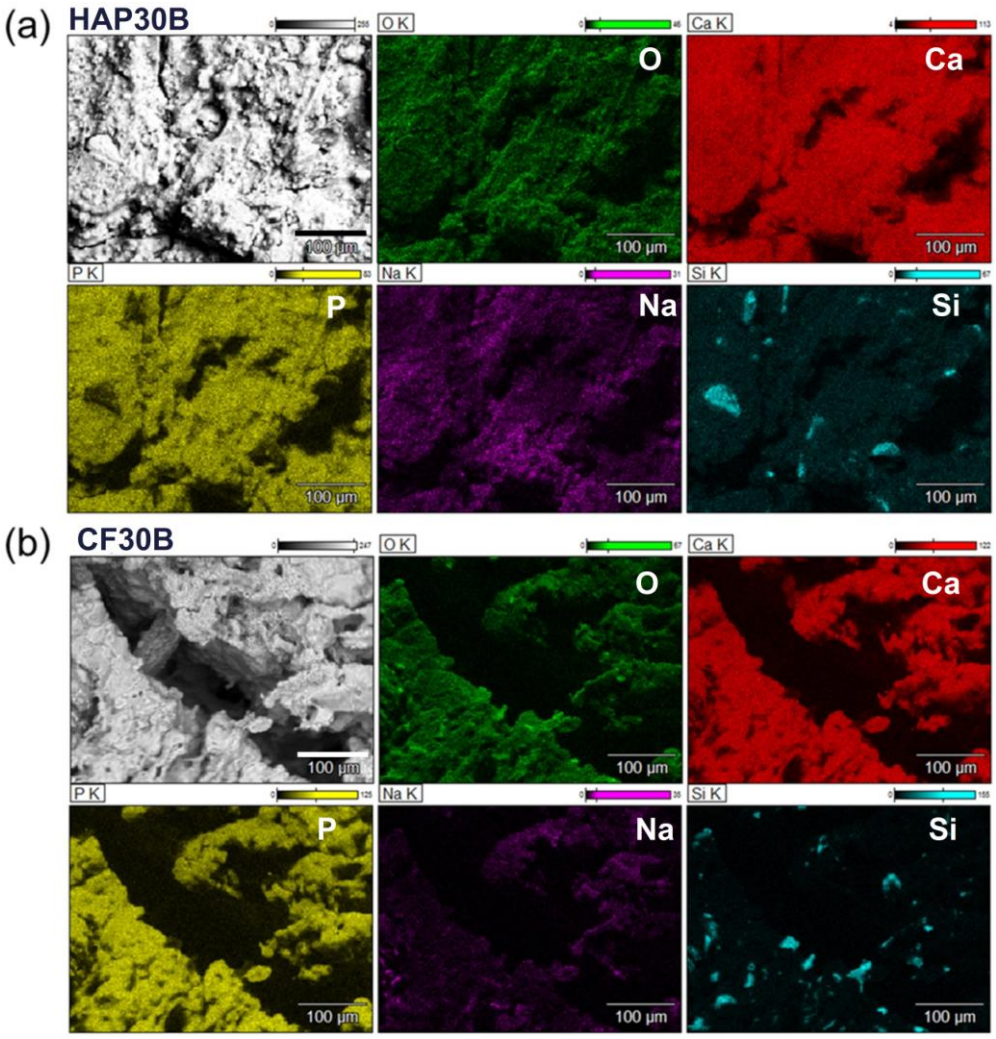

Figure 4. EDXS element mapping of the specimens after the thermal treatment at 900°C: (a) samples HAP30B; (b) samples CF30B. Scale bars in the figures are equivalent to 100 µm.

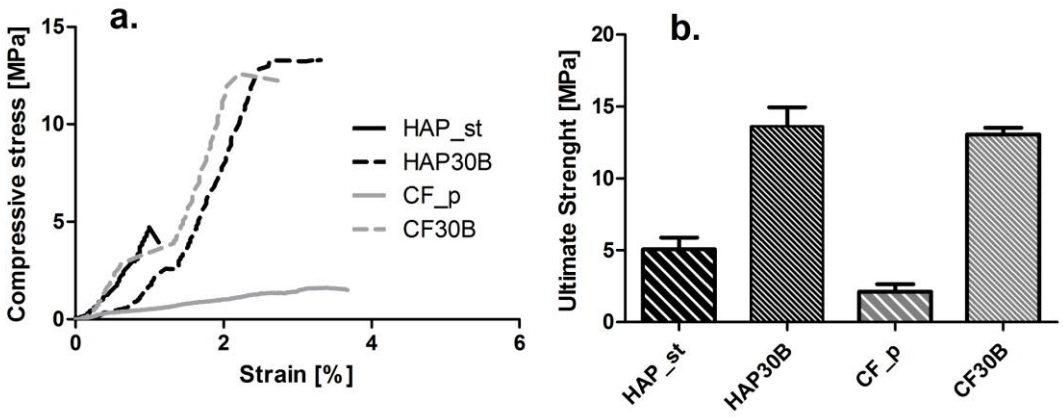

Figure 5. Mechanical behavior of the different samples (HAP_st, HAP30B, CF_p and CF30B) subjected to uniaxial compression; (a) Representative stress-strain curves (b) Ultimate compressive strength. (*) $p < 0.001$.

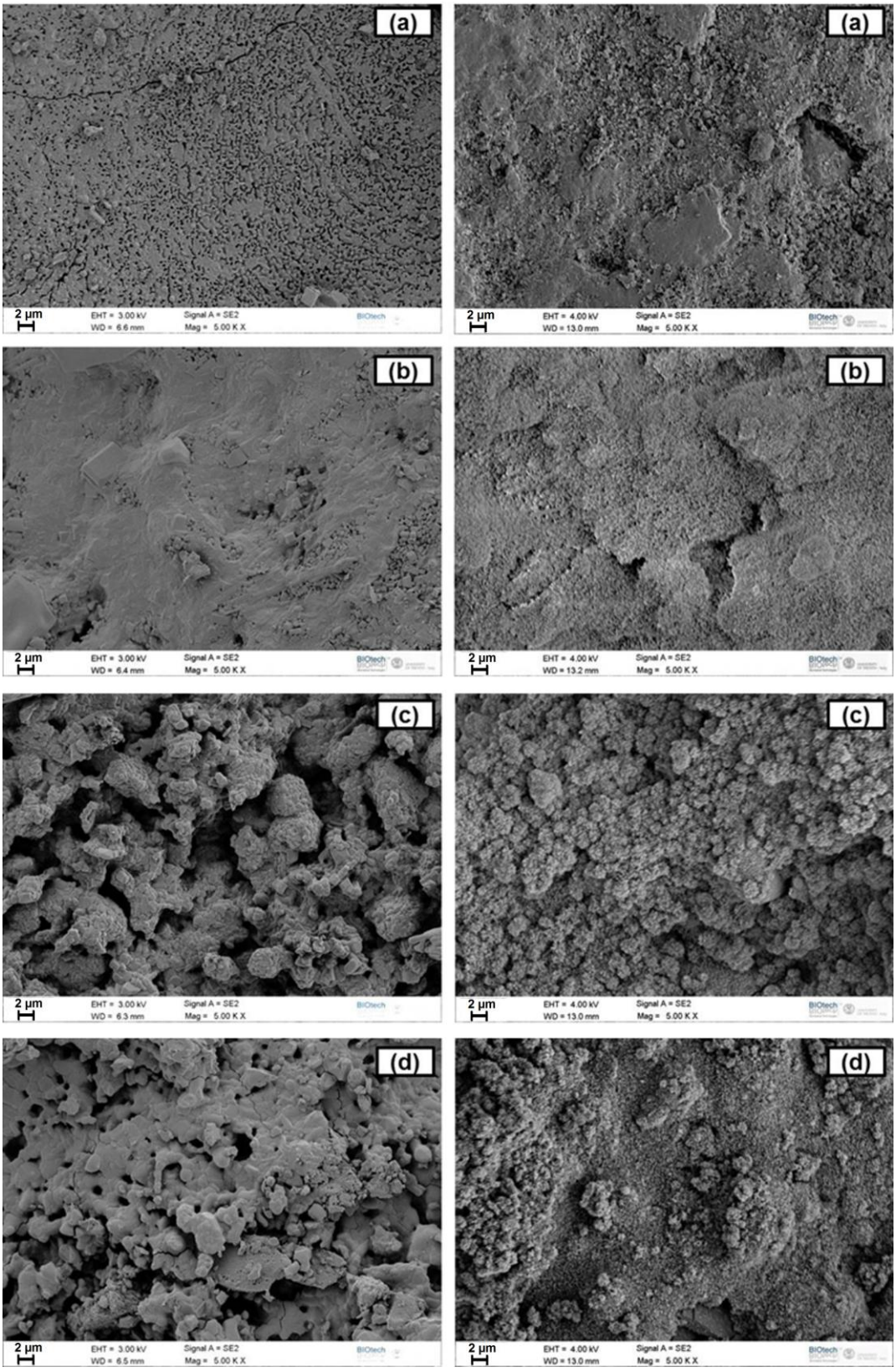

Figure 6. Secondary electron scanning micrographs of the different bioceramic formulations: (a) samples HAP_st, (b) samples HAP30B, (c) samples CF_p, (d) samples CF30B, before (left) and after (right) incubation in DMEM for 7 days .

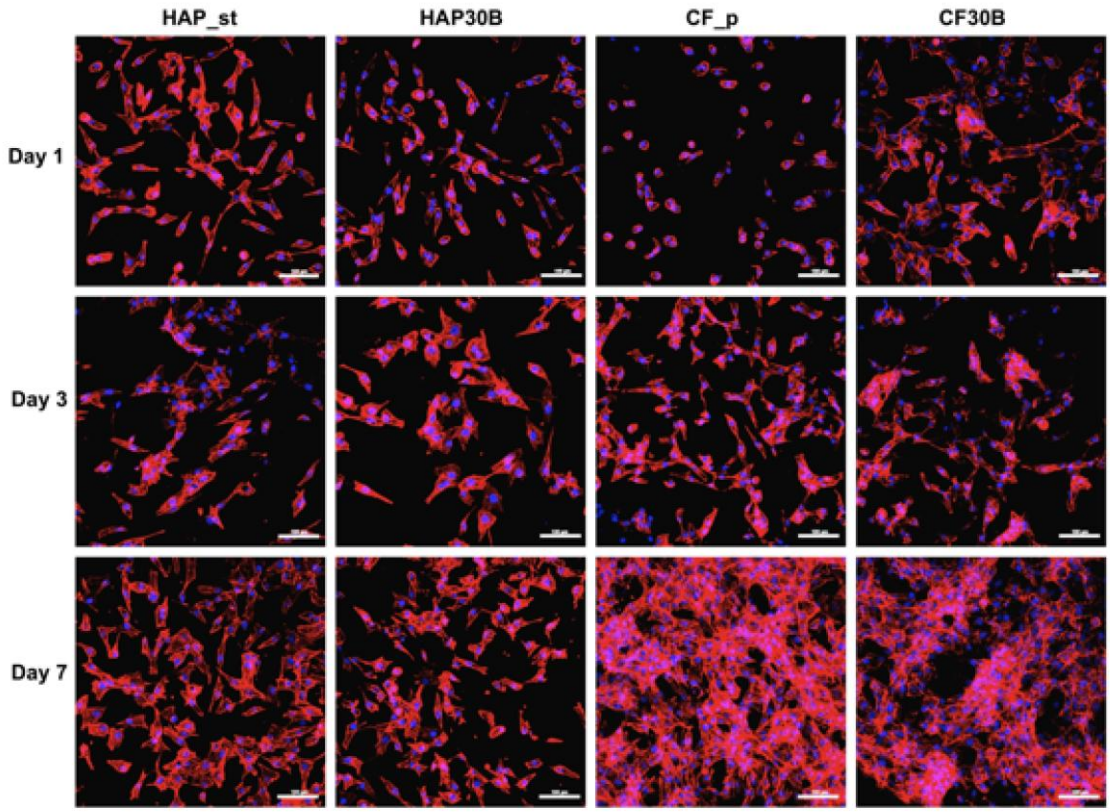

Figure 7. Rhodamine-labeled phalloidin (F-actin fibers in red) and DAPI (nuclei, blue) were used to visualize cell cytoskeleton organization and cell distribution of MG63 cells cultured for 1, 3 and 7 days on samples: HAP_st, HAP30B, CF_p and CF30B. Scale bars in the figures are equivalent to 100 μm.

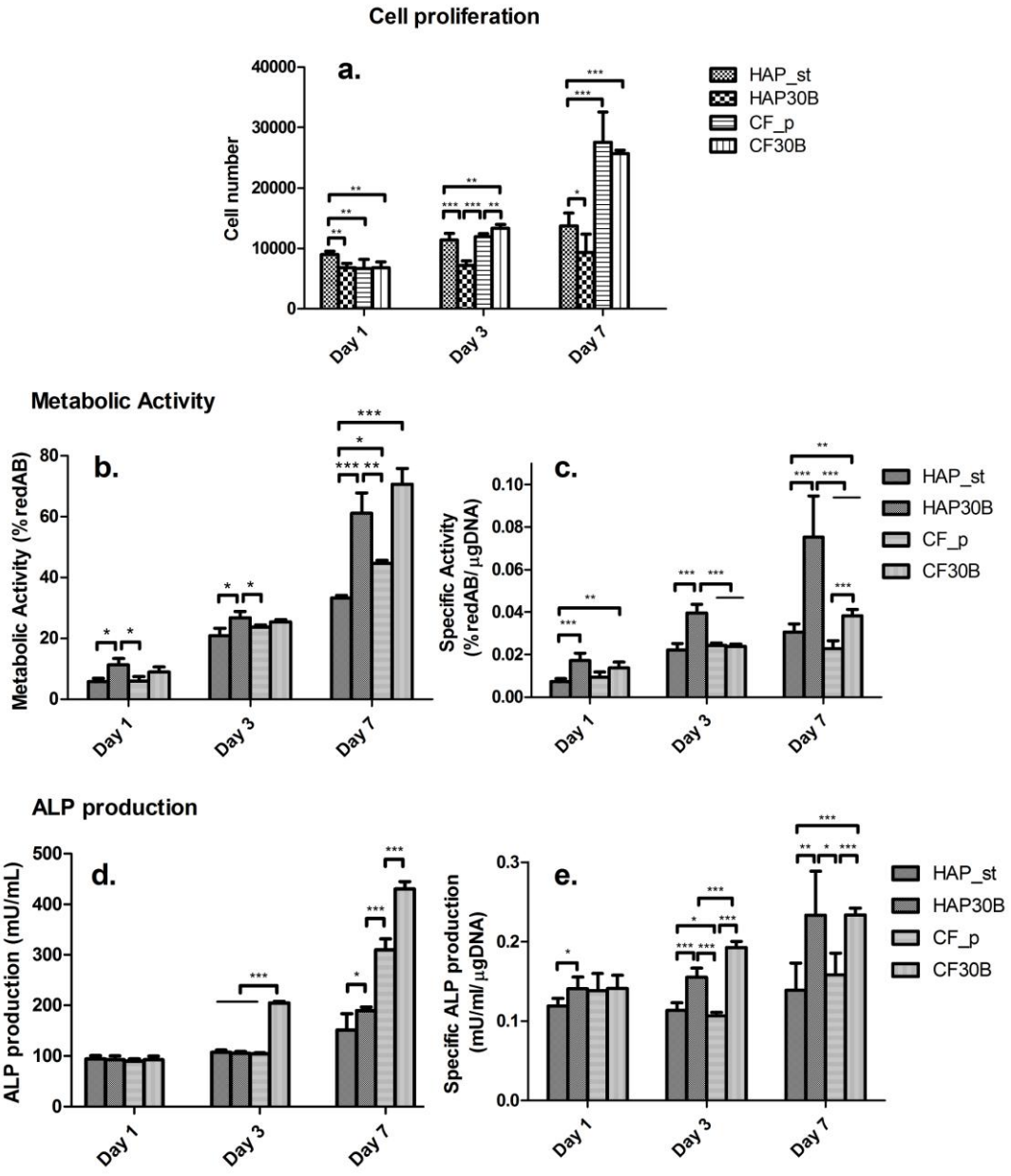

Figure 8. Adhesion, proliferation, metabolic activity and ALP production for MG63 cells cultured for 1, 3 and 7 days on the surface of the bioceramic samples (HAP_st, HAP30B, CF_p and CF30B); (a) Cell number derived from total DNA content measured by PicoGreen® quantification assay, (b) Total metabolic activity determined by AlamarBlue® assay, (c) Metabolic activity was normalized with respect to DNA content, (d) Total ALP production determined alkaline phosphatase test, (e) ALP production normalized with respect to DNA content. All the data were presented as mean ±SD. (*) $p < 0.05$, (**) $p < 0.01$, (***) $p < 0.001$.